Journal of Biomechanics

Mitigation Effect of Cell Exclusion on Blood Damage in Spiral Groove Bearings

--Manuscript Draft--

Manuscript Number:	BM-D-22-00396R3
Article Type:	Full Length Article (max 3500 words)
Keywords:	Left ventricular assist device, spiral groove bearing, cell exclusion, haemolysis, HMW vWF multimer degradation
Corresponding Author:	Chris Hoi Houng Chan, Ph.D Griffith University Brisbane, QLD AUSTRALIA
First Author:	Chris Hoi Houng Chan, Ph.D
Order of Authors:	Chris Hoi Houng Chan, Ph.D
	Tomotaka Murashige
	Shelby A. Bieritz
	Clayton Semenzin
	Amanda Smith
	Laura Leslie
	Michael J. Simmonds
	Geoff D. Tansley
Abstract:	Cell exclusion in spiral groove bearing (SGB) excludes red blood cells from high shear regions in the bearing gaps and potentially reduce haemolysis in rotary blood pumps. However, this mechanobiological phenomenon has been observed in ultra-low blood haematocrit only, whether it can mitigate blood damage in a clinically-relevant blood haematocrit remains unknown. This study examined whether cell exclusion in a SGB alters haemolysis and/or high-molecular-weight von Willebrand factor (HMW vWF) multimer degradation. Citrated human blood was adjusted to 35% haematocrit and exposed to a SGB (n=6) and grooveless disc (n=3, as a non-cell exclusion control) incorporated into a custom-built Couette test rig operating at 2000RPM for an hour; shearing gaps were 20, 30, and 40 μm. Haemolysis was assessed via spectrophotometry and HMW vWF multimer degradation was detected with gel electrophoresis and immunoblotting. Haemolysis caused by the SGB at gaps of 20, 30 and 40μm were 10.6±3.3, 9.6±2.7 and 10.5±3.9 mg/dL.hr compared to 23.3±2.6, 12.8±3.2, 9.8±1.8 mg/dL.hr by grooveless disc. At the same shearing gap of 20 μm, there was a significant reduced in haemolysis (P=0.0001) and better preserved in HMW vWF multimers ($p<0.05$) when compared SGB to grooveless disc. The reduction in blood trauma in the SGB compared to grooveless disc is indicative of cell exclusion occurred at the gap of 20μm. This is the first experimental study to demonstrate that cell exclusion in a SGB mitigates the shear-induced blood trauma in a clinically-relevant blood haematocrit of 35%, which can be potentially utilised in future blood pump design.

Mitigation Effect of Cell Exclusion on Blood Damage in Spiral Groove Bearings

Short title: Can Cell Exclusion Reduce Blood Damage?

Chris Hoi Houng Chan[+1, 2], Tomotaka Murashige[+1, 3], Shelby A. Bieritz[1, 4], Clayton Semenzin[1, 2], Amanda Smith[5], Laura Leslie[6], Michael J. Simmonds[5] and Geoff D. Tansley[1, 2]

[1]School of Engineering and Built Environment, Griffith University, Queensland, Australia;
[2]Critical Care Research Group, The Prince Charles Hospital, Brisbane, Australia;
[3]School of Engineering, Tokyo Institute of Technology, Meguro, Japan;
[4]Department of Bioengineering, Rice University, Houston, TX, USA;
[5]Menzies Health Institute Queensland, Griffith University, Queensland, Australia;
[6]Mechanical, Biomedical and Design Group, Aston University, Birmingham, UK.

[+] Chris H.H. Chan and Tomotaka Murashige contributed equally to this work

Corresponding author:

Dr. Chris Chan Hoi Houng

Griffith University

Critical Care Research Group

Clinical Sciences Building, Level 3

The Prince Charles Hospital

Chermside, QLD 4032

Email: chris_houng@hotmail.com

Tel: +61 424 887 256

Key Words: Left ventricular assist device, spiral groove bearing, cell exclusion, haemolysis, HMW vWF multimer degradation

Mitigation Effect of Cell Exclusion on Blood Damage in Spiral Groove Bearings

Cell exclusion in spiral groove bearing (SGB) excludes red blood cells from high shear regions in the bearing gaps and potentially reduce haemolysis in rotary blood pumps. However, this mechanobiological phenomenon has been observed in ultra-low blood haematocrit only, whether it can mitigate blood damage in a clinically-relevant blood haematocrit remains unknown. This study examined whether cell exclusion in a SGB alters haemolysis and/or high-molecular-weight von Willebrand factor (HMW vWF) multimer degradation. Citrated human blood was adjusted to 35% haematocrit and exposed to a SGB (n=6) and grooveless disc (n=3, as a non-cell exclusion control) incorporated into a custom-built Couette test rig operating at 2000RPM for an hour; shearing gaps were 20, 30, and 40 μm. Haemolysis was assessed via spectrophotometry and HMW vWF multimer degradation was detected with gel electrophoresis and immunoblotting. Haemolysis caused by the SGB at gaps of 20, 30 and 40μm were 10.6±3.3, 9.6±2.7 and 10.5±3.9 mg/dL.hr compared to 23.3±2.6, 12.8±3.2, 9.8±1.8 mg/dL.hr by grooveless disc. At the same shearing gap of 20 μm, there was a significant reduced in haemolysis (P=0.0001) and better preserved in HMW vWF multimers ($p<0.05$) when compared SGB to grooveless disc. The reduction in blood damage in the SGB compared to grooveless disc is indicative of cell exclusion occurred at the gap of 20μm. This is the first experimental study to demonstrate that cell exclusion in a SGB mitigates the shear-induced blood damage in a clinically-relevant blood haematocrit of

35%, which can be potentially utilised in future blood pump design.

Introduction

Due to the limited availability of donor hearts, left ventricular assist device (LVAD) therapy provides another alternative life-saving solution to many end-stage heart failure patients who would not otherwise survive while on the heart transplant waiting list (Molina et al., 2021). Third generation LVADs, comprising of contact-free magnetic or hydrodynamic bearings, have nearly superseded first generation volume displacement and second generation contact bearing devices due to enhanced durability and haemocompatibility (Kirklin et al., 2015; Mehra et al., 2018; Mehra et al., 2017; Rogers et al., 2017). Magnetic bearings allow for wide blood-flow gaps and lower shear stress, thus enhancing haemocompatibility (Bourque et al., 2016; Krabatsch et al., 2017; Uriel et al., 2017). Nonetheless, an active magnetic bearing needs additional sensors, power input, and a highly sophisticated control mechanism for stable suspension, which increases the system's complexity and power consumption. Hydrodynamic bearing may offer an alternative solution to these problems (Fu et al., 2019). To develop a miniature LVAD, a hydrodynamic bearing has the advantage of maximum load capacity with minimum space requirements compared to active magnetic bearing because they are passive and do not require additional space for electrical control elements (Kink and Reul, 2004). However, narrow bearing gap in hydrodynamic bearings are required for dynamic

74 pressure buildup to support bearing load, which leads to high mechanical shear stress that
75 may initiate blood damage (Blackshear et al., 1966; Leverett et al., 1972).
76
77 The spiral groove bearing (SGB) is a unique hydrodynamic bearing, which features an
78 excellent load capacity. Cell exclusion occurrence in SGB has been long discussed and
79 investigated, which can potentially minimise blood cell exposure to high mechanical
80 shear stress that may initiate blood damage. Kink *et al.* (Kink and Reul, 2004) first
81 assumed that no blood cells enter the bearing gap once the SGB is spinning in an axial
82 blood pump due to cell exclusion, with supporting results of flow visualisation
83 experiments on a 10 : 1 scale-up model. Later on, Leslie *et al*. observed that cell exclusion
84 occurs in a SGB incorporated into a custom-built rig, leading to lower haematocrit and
85 blood viscosity at the high shear ridge surface in a gap of 25 μm using ultra-low blood
86 haematocrit of less than 1 % (Leslie et al., 2013). Further on, Murashige showed that cell
87 exclusion occurs in the SGB of hydrodynamic bearing blood pumps, with less than 30
88 μm bearing gap using blood haematocrit of 1% (Murashige et al., 2016). To prove the
89 existence of cell exclusion in a SGB while maintaining a clinically-relevant haematocrit,
90 we previously demonstrated that the cell exclusion occurs in SGB, which incorporated in
91 the current custom-built Couette test rig with the same operating conditions using 35%
92 blood haematocrit of fluorescently-tagged erythrocyte ghost cells and visualised by a
93 particle image velocimetry (Bieritz, 2020). However, the ability of mitigation effect of

cell exclusion on blood damage in SGB remains questionable. Therefore, the aim of this study was to investigate whether cell exclusion in a SGB using clinically-relevant blood haematocrit of 35 %, can reduce blood damage such as haemolysis and high molecular weight von Willebrand factor (HMW vWF) multimer degradation using the same developed test rig.

Materials and methods

Blood collection

Fresh human whole blood (300 mL) was collected from healthy volunteers, and anticoagulated with citrate phosphate dextrose adenine (CPDA-1) solution (Terumo Corporation, Tokyo, Japan). Written, informed consent was obtained from participating volunteers. The blood haematocrit was adjusted to 35 ± 1 % with autologous plasma obtained from spared blood after centrifuged at 2330 × g for 45 minutes at 4°C. The experimental protocols were reviewed and approved by the Griffith University Human Research Ethics Committee (Protocol number 2018/633).

A custom-built Couette test rig

The mitigation effect of cell exclusion on blood damage in a SGB was investigated using a custom-built Couette test rig as shown in Figure 1a. This test rig comprised of an acrylic reservoir with inlet and outlet connectors, a force sensor (Nano43; ATI Industrial

114 Automation, Apex, NC, USA), a motor-driven bearing, a polyvinyl chloride tubing
115 (Tygon S3 E-3603, Saint Gobain, Courbevoie, France), a flow sensor (4PXN; Transonic
116 Systems Inc., Ithaca, NY, USA), a sampling port connected to the outlet connector, and a
117 z-axis translation stage (ZLPG60; MISUMI Group Inc., Tokyo, Japan).
118
119 The SGB was milled from cast acrylic and subsequently vapor polished, with the ridge
120 surface of the bearing masked to preserve the square edges between the groove walls and
121 ridge surface. The SGB geometry was: outer diameter 44.8 mm, inner diameter 12.35 mm,
122 groove depth 200 μm, groove angle 16°, number of grooves 15, and the ridge to groove
123 width ratio was 1:1 (Figure 1b). The acrylic reservoir was mounted to the z-axis
124 translation stage with a 5 μm resolution, so that the shearing gap between the bottom
125 surface of the blood reservoir and the ridge surface of the SGB could be adjusted precisely.
126 To set the shearing gap, the reservoir was raised using the z-axis stage until bearing
127 touchdown was detected by a change in z-axis force. Bearing touchdown was measured
128 at 6 bearing angular positions, and each measurement was repeated twice to ensure
129 repeatability. The average touchdown stage position was set as the zero point prior to each
130 experiment. The touchdown stage position had a variance of 11 μm, thus the zero point
131 had a tolerance of ± 5.5 μm. As a SGB rotates, primary blood flow is driven against the
132 groove wall opposite to the direction of rotation, which builds pressure in the
133 circumferential direction across the width of each groove. These local regions of high

pressure may prevent red blood cells from flowing into the adjacent ridge as the SGB rotates. Because the groove depth bearing generates primary flow rates, a higher pressure buildup occurs across each groove.

Prior to each blood test, the circulation loop was rinsed with phosphate buffered saline (Sigma–Aldrich, St. Louis, MO, USA) for 20 minutes. Blood was subsequently introduced into the circuit (total blood volume in the circuit, 45 ± 5 mL) and circulated for an hour in each gap at room temperature. The SGB was rotated at 2000 revolutions per minute (RPM). Blood samples (1.5 mL) were collected at baseline (5 minute) and an hour from the sampling port connecting to the outlet connecter. The shearing gaps were set to 20, 30 and 40 μm for each test using the same donor's blood to eliminate the risk of the individual variability. The SGB force and flow rate were measured throughout all experiments, and the data was acquired using an acquisition system (MicroLabBox; dSPACE GmbH, Paderborn, Germany) and MATLAB Simulink (R2016b; The MathWorks Inc., Natick, MA, USA).

Control tests using grooveless disc and same flow rate using clamp

To study the shearing gap effect without cell exclusion, a grooveless disc with the same diameter of the SGB was used as a control. Blood was filled into the circulation loop. The rotational speed of the grooveless disc was set to 2000 RPM for an hour and the shearing

gaps were set to 20, 30 and 40 μm, respectively.

An additional control study was performed to eliminate the confounding effect of flow rate on haemolysis in different shear gaps (Blackshear et al., 1966; Leverett et al., 1972). This control measure was taken because as the SGB gap decreases (40 μm, 30 μm, 20 μm), the flow rate increases (40 mL/min, 50 mL/min, 60 mL/min). To isolate the effects of flow rate on haemolysis, the flow rate was set to a constant in different gaps of 30 μm and 20 μm gap for two hours. For the 20 μm gap, the outflow of the fluid reservoir was clamped until the flow rate reached 50 mL/min (versus the unclamped 60 mL/min), which matching the flow rate at 30 μm gap (50 mL/min).

Haemolysis assay

The Harboe assay was used for quantifying haemolysis as previously (Chan et al., 2022). The 1.5 mL blood samples at baseline and an hour were centrifuged at 1500 × *g* for 10 minutes to obtain plasma, which was then diluted in 0.1 % Na_2CO_3 (1:10), and the absorbance of each sample was measured at 380, 415 and 450 nm using a spectrophotometer (UVmini-1240; Shimadzu Corp., Kyoto, Japan). The plasma-free haemoglobin (*pf*Hb) was calculated as described by the equation below where A_x is the absorbance of x nm wavelength. The triplicated measurement was done in this measurement.

$$pf\text{Hb}\ (\frac{\text{mg}}{\text{dL}}) = (167.2 \times A_{415} - 83.6 \times A_{380} - 83.6 \times A_{450}) \times (\frac{1}{10}) \times (\frac{1}{dilution\ in\ 0.1\%\ Na2CO3})$$

vWF multimer analysis

The remaining plasma samples were further centrifuged at 15,000 × *g* for 5 minutes. Platelet-poor plasma (PPP) was stored at −80°C for further vWF multimer analysis. Gel electrophoresis was performed as previously described (Chan et al., 2020; Chan et al., 2017). Briefly, PPP prepared from sheared samples was thawed and centrifuged at 15 000× *g* for 5 minutes to remove debris. Then, 10 µL of PPP was loaded into each well, and subjected to electrophoresis using high gelling temperature agarose (50040, Lonza, Basel, Switzerland). The gel comprised of a 0.8 % stacking gel and a 1.5 % running gel. Electrophoresis was performed at room temperature for 20 hours at 60 voltages and for 4 hours at 80 voltages. The fractionated plasma proteins were then transferred from the gel to a polyvinylidene difluoride membrane (0.45 mm, IPVH304F0, Immobilon-P, Millipore Corporation, Billerica, MA, USA) using capillary blotting method. Membrane was blocked using 5 % skim milk in Tris Buffered Saline with Tween (Sigma Aldrich, St. Louis, MO., USA) and probed with horseradish peroxidase conjugated polyclonal rabbit anti-human vWF (1:1000) (P0226, DAKO, Glostrup, Denmark). Membranes were washed and developed with enhanced chemiluminescence (Clarity™ ECL Western Blotting Substrate, Bio-Rad Laboratories Inc, Hercules, CA, USA), and vWF multimer band density visualised with a ChemiDoc Imaging Systems (ChemiDoc™ MP, Bio-Rad

Laboratories Inc, Hercules, CA, USA). The HMW multimer degradation within subject was quantified using a ratio of HMW vWF multimers (> band 10) at an hour compared to the baseline sample. Similarly, changes in low molecular weight von Willebrand factor (LMW vWF) multimer profiles within subject were quantified using a ratio of LMW vWF multimers (band 1-5) at an hour compared to the baseline sample. The molecular weight vWF multimers were quantified using standard software (Image LAB 6.1, Bio-Rad Laboratories Inc, Hercules, CA, USA).

Computational fluid dynamics

To support the experimental findings, a steady-state computational fluid dynamics (CFD) simulation of the SGB was conducted using ANSYS Fluent (2020 R2, ANSYS Inc., Canonsburg, PA, USA). A single groove and ridge segment was modelled, and periodic boundary conditions were utilised to represent the full bearing. Preliminary simulations determined a mesh density of approximately 1.9 million cells was sufficient to reach a mesh independent solution. The flow field was treated as laminar flow.

Statistical analysis

Haemolysis was analysed using a 2-way ANOVA method for statistical analysis (mean ± standard deviation). The increases in *pf*Hb for 20 μm gap with the clamp and 30 μm gap without the clamp were compared using a paired t-test for statistical evaluation. The ratio

of HMW vWF and LMW vWF multimers between baseline and an hour were compared between different shearing gaps and two different geometries using a 2-way ANOVA analysis. All statistical analysis was performed using GraphPad Prism 9.0 software (GraphPad Software, San Diego, CA, USA).

Results

Haemolysis level

The release of *pf*Hb in 20, 30 and 40 μm in the SGB after an hour were 10.6 ± 3.3, 9.6 ± 2.7, and 10.5 ± 3.9 mg/dL.hr, respectively (n= 6, Figure 2). There was no significant difference in haemolysis measured in SGB after an hour among these shearing gaps. Whereas, the release of *pf*Hb in 20, 30 and 40 μm in the grooveless disc after an hour were 23.3 ± 2.6, 12.8 ± 3.2, 9.8 ± 1.8 mg/dL.hr, respectively (n= 3, Figure 2). There was significant difference in haemolysis measured in grooveless disc after an hour when using the 20 μm gap compared with the 30 μm ($P = 0.0007$) and 40 μm ($P < 0.0001$). Comparing the SGB and grooveless disc at equal shearing gap, there was a significant difference in *pf*Hb after an hour of exposure in the 20 μm gap ($P = 0.0001$).

There was no significant difference in haemolysis after two hours of exposure time between the clamp and unclamped conditions when both flow rates were set at 50 mL/min (n= 3, Figure 3). The release of *pf*Hb in 20 μm with the clamp compared to 30 μm with

no clamp were 13.4 ± 5.4 and 11.3 ± 8.9 mg/dL.hr, respectively.

Quantification of the degradation of HMW vWF multimers and accumulation of LMW vWF multimers

In Figure 4a, vWF multimer analysis revealed that HMW vWF multimers were degraded into either intermediate or LMW vWF multimers after an hour, for both the SGB and grooveless disc. In Figure 4b, no significant differences were found for HMW vWF ratios of baseline and an hour among shearing gaps of 20-40 μm using either SGB or grooveless disc. However, at the same shearing gap of 20 μm, the grooveless disc had significantly reduced HMW vWF ratios of baseline and an hour when compared with the SGB ($p < 0.05$). In Figure 4c, no significant differences were found for LMW vWF ratio of baseline and 60 minutes among shearing gaps of 20-40 μm using either a SGB or grooveless disc. There were also no signficant difference for LMW vWF ratio of baseline and an hour between grooveless disc and SGB at any testing gaps between 20-40 μm.

CFD analysis

The simulation results showed that the majority of the flow (primary flow) travels along the grooves as demonstrated by the streamlines in Figure 5. Flow in the ridge regions travelled towards the grooves (secondary flows) where it then joined the primary flow. In Figure 6, the shear stress contour plot from a cross-section of the groove and ridge

demonstrated that the ridge region generated higher shear stress than the groove region of the bearing.

Discussion

Plasma skimming occurs physiologically with the separation of plasma and red blood cells (RBC), which occurs at diverging bifurcations, leading to a heterogeneous RBC distribution that ultimately affects the oxygen delivery to living tissues (Fåhræus and Lindqvist, 1931). A similar mechanobiological mechanism in cell exclusion, RBCs moving from areas of high shear to low shear, observed in SGB using low blood haematocrit only (Leslie et al., 2013; Murashige et al., 2016). We previously demonstrated that the cell exclusion occurs in SGB in the current developed test rig using 35% blood haematocrit of fluorescently-tagged erythrocyte ghost cells and visualised by a particle image velocimetry (Bieritz, 2020). As to continue this work, we further evaluated and completed the investigation of the ability of mitigation effect of cell exclusion on blood damage in SGB, with some additional CFD support. Therefore, this study demonstrated that cell exclusion can reduce blood damage in a SGB using clinically-relevant blood haematocrit of 35 %.

We assumed that flowing blood between the narrow bearing gaps behave as (1) Newtonian fluid (2) Couette flow (3) did not consider for entrance effects and microfluid

mechanics. Based on these assumptions, we calculated the maximum ridge surface shear stress, τ_{ridge} and maximum groove shear stress, τ_{groove} at outer diameter of the SGB based on equations (1) and (2), which has used by previous works (Kosaka et al., 2021; Murashige et al., 2015) as follows

$$\tau_{ridge} = \mu \times \frac{V_c}{h_{gap}} \quad - \quad (1)$$

$$\tau_{groove} = \mu \times \frac{V_c}{h_{groove}} \quad - \quad (2)$$

Where μ is blood viscosity (3.0 mPa·s; typical of asymptotic values), V_c is the outer circumferential velocity of the rotor ($r \times \omega_c$), h_{gap} is the shearing gap, h_{groove} is the groove gap (h_{gap} + 200 μm), r is the radius of the SGB (22.4 mm), ω_c is the outer circumferential angular speed of the rotor ($2\pi \times \frac{2000\ RPM}{60}$). τ_{ridge} in the shearing gap of 20, 30 and 40 μm were calculated as 704, 469 and 352 Pa, respectively. τ_{groove} in the groove shearing gap of 220, 230 and 240 μm were calculated as 64, 61 and 59 Pa, respectively (See Table 1). Re_{ridge} is the pump Reynolds number at ridge regime (Malinauskas et al., 2017) and Re_{groove} is the pipe flow Reynolds number at groove regime. Based on the calculated Reynolds number equations (3) and (4), both ridge and groove flow regimes are considered laminar flow due to both Reynolds numbers are below Critical Reynolds numbers, see Table 1 (Note that: for Re_{ridge}, Critical Reynolds number is found based on

289 gap ratio, G = h_{gap} / r versus Reynolds number, (Daily J and Nece R, 1960)).

$$Re_{ridge} = \frac{\rho \times \omega_C \times D^2}{\mu} \quad - \quad (3)$$

$$Re_{groove} = \frac{\rho \times u_{gap} \times d_H}{\mu} - \quad (4)$$

290 Where ρ is the blood density (1060 kgm^{-3}), D is the diameter of the SGB (44.8 mm), u_{gap}
291 is the average blood flow speed within each groove (Q_{gap} / $Area_{groove}$ × 15), Q_{gap} is the
292 measured volumetric flow rate, $Area_{groove}$ is the area of groove (a × b, where groove depth,
293 a = 0.2 mm and groove width, b = 3 mm) and d_H is the open channel hydraulic diameter
294 (4ab / 2a+b). Chan *et al.* reported that a significant increase in haemolysis can be observed
295 when shear stress is higher than 90 Pa using Couette-type blood-shearing devices (Chan
296 et al., 2022). Therefore, increased haemolysis in the SGB ridge region and grooveless
297 disc (≥ 352 Pa) is expected as the estimated shear stress is higher than 90 Pa. When the
298 shearing gaps reducing from 40 μm to 20 μm, the calculated shear stress in these shearing
299 gaps of SGB surface ridges and grooveless disc both increased by 100 % (352 Pa to 704
300 Pa), whereas the SGB groove gaps increased by only 8.5 % (59 Pa to 64 Pa). At the same
301 shearing gap of 20 μm, the calculated shear stress in the shearing gap of SGB surface
302 ridges and grooveless disc are 11-fold higher than in the SGB grooves (704 Pa versus 64
303 Pa). Interestingly, our results showed that no change in haemolysis as the SGB gap

304 reducing from 40 to 20 μm. This finding suggests RBC entrainment in the low-shear
305 groove ($\tau_{groove} \leq 64$ Pa), rather than exposure to the higher-shear surface ridge regions
306 ($\tau_{ridge} \geq 352$ Pa).
307
308 The CFD plots suggested that particles in the high shear region of the ridge migrate
309 towards the low shear regions of the grooves. Our CFD model did not account for the
310 Fåhraeus effect, therefore the result is expected to be more exaggerated. Blood was treated
311 as Newtonian fluid and the fluid modelled as homogeneous (RBC aggregation were not
312 take into consideration). The limitations would influence the finer details of the simulated
313 results; however, the bulk flow patterns of interest would be negligibly impacted. Overall,
314 the CFD findings strongly support the haemolysis results indicating cell exclusion effect
315 in SGB. In Figure 7, the surface-shear stress analysis image of the SGB demonstrates as
316 a visual guide that the local rise in differential pressure across the ridge surface excludes
317 red blood cells to low shear regions within the grooves.
318
319 Our previous work also demonstrated that haematocrit decreased at the ridge surface of
320 SGB when the gap was less than 30 μm due to cell exclusion occurred in a SGB of the
321 blood pump (Murashige et al., 2016). Therefore, a SGB has the ability to reduce
322 haemolysis by excluding the RBCs from area of high shear stress to the low shear stress
323 of the bearing grooves, thus mitigating shear-induced haemolysis in the narrow bearing

gap required in the hydrodynamic bearing. Cell exclusion in SGBs acts as an effective protection of the RBCs by reducing the exposure time at high-shear regional ridges, excluding RBCs to the low shear regional grooves. Therefore, our current findings substantiate the previous claims that narrow bearing gaps between the impeller blades, tips and pump housing generate supraphysiological shear stress in previous rotary blood pumps; yet, produced low haemolysis maybe due to cell exclusion effect (Antaki et al., 2008; James et al., 2003). As the shearing gap decreases led to increase in flow rate, hence the change in haemodynamic profile, might lead to blood damage. However, the result in Figure 3 confirmed that flow rate had an insignificant influence on haemolysis even up to 2 hours in these SGB geometries. Therefore, we did not adjust the flow rate throughout the study since the flow rate is not the significant influencing factor in this study.

It is well known that supraphysiologic shear stress can cause pathologic vWF degradation during LVAD support and lead to acquired von Willebrand syndrome (Crow et al., 2010; Crow et al., 2009). Recently, Bartoli *et al.* reported that specifically designed low shear stress LVADs can reduce HMW vWF multimer degradation (Bartoli et al., 2019; Bartoli et al., 2020). So far, no work has been reported on whether cell exclusion can reduce vWF degradation. Although our results showed that SGB preserves more HMW vWF multimers compared to grooveless disc at shear gap of 20 μm. However, both geometries caused significant HMW vWF multimer degradation due to the calculated shear stresses

ranging from 59 Pa to 704 Pa, which are well beyond previously claimed shear stress maximum threshold of 12 Pa for vWF. Thus, high shear was likely to be the cause of HMW vWF multimer degradation and LMW vWF multimer accumulation (Chan et al., 2020; Chan et al., 2022). When blood is exposed to a high shear environment, the interaction between RBC-vWF is weak (Smeets et al., 2017) and the mechanobiological response of RBCs and vWF are uniquely different. Due to the excellent property to deform, the RBC is able to squeeze reversibly and escape to lower shear areas (i.e., cell exclusion) (Huisjes et al., 2018), whereas vWF proteins unfold under shear, adhering and constituting a "sticky" grid necessary for blood platelet adhesion (Schneider et al., 2007). Therefore, the cell exclusion in SGB might not be fully protective to vWF degradation.

Limitations

This custom-built Couette test rig enabled us to systematically investigate the effects of cell exclusion in a SGB on blood damage such as haemolysis and HMW vWF multimer degradation. However, our study has a number of limitations. First, we must emphasise that the haemolysis results of grooveless disc cannot be directly compared to SGB due to the distinctly different flow patterns generated by the two geometries. The rotating grooveless disc creates a flow driven radially outward by centrifugal force, whereas the SGB draws fluid spirally inward to the central of the bearing. Second, although our test results showed that cell exclusion can reduce blood damage, however, the sample size

and test duration were relatively small and short. Therefore, these test results might affected by the blood donor variability and measurement error. Unfortunately, our rig had been dismantled and no longer able to re-examine the blood trauma test for a longer test time or more tests. Lastly, this work did not investigate the cell exclusion effect on platelets and leukocytes, which are important for overall haemocompabitlity of new development of LVADs.

Conclusion

Our experimental results indicate that the cell exclusion in the SGB can reduce haemolysis, but might not be fully protective to HMW vWF multimer degradation. Our results also showed that cell exclusion occurred in a clinically-relevant blood haematocrit of 35 %, which removes the doubt of it only occurring in ultra-low blood haematocrit. This finding suggests that the cell exclusion effect in a SGB can be potentially utilised and improved the haemocompatibility of a small geometry pump design such as a miniature, percutaneous and paediatric LVAD.

Acknowledgement

Chris H.H. Chan is supported by The Prince Charles Hospital Foundation Research Fellowship (RF2019-02). Tomotaka Murashige is supported by a Grant-in-Aid for Japan Society for the Promotion of Science Fellow (17J08128). The authors would like to

recognise the financial assistance provided by The Prince Charles Hospital Foundation Team Grant (TM2017-04) and Innovation Grant (INN2021-06).

Authors' contributions

- Chan: Concept/design, analysis/data interpretation, secured funding, drafting/critical revision/approval of article;
- Murashige: Concept/design, analysis/data interpretation, secured funding, drafting/critical revision/approval of article;
- Bieritz: Concept/design, analysis/data interpretation, secured funding, drafting/critical revision/approval of article;
- Semenzin: CFD analysis/data interpretation, critical revision/approval of article;
- Smith: Statistical analysis, critical revision/approval of article;
- Leslie: Critical revision/approval of article;
- Simmonds: Concept/design, critical revision/approval of article;
- Tansley: Concept/design, critical revision/approval of article.

Reference

Antaki, J.F., Diao, C.G., Shu, F.J., Wu, J.C., Zhao, R., Kameneva, M.V., 2008. Microhaemodynamics within the blade tip clearance of a centrifugal turbodynamic blood pump. Proceedings of the Institution of Mechanical Engineers. Part H, Journal of engineering in medicine 222, 573-581.

Bartoli, C.R., Hennessy-Strahs, S., Gohean, J., Villeda, M., Larson, E., Longoria, R., Kurusz, M., Acker, M.A., Smalling, R., 2019. A Novel Toroidal-Flow Left Ventricular Assist Device Minimizes Blood Trauma: Implications of Improved Ventricular Assist Device Hemocompatibility. The Annals of thoracic surgery 107, 1761-1767.

Bartoli, C.R., Kang, J., Motomura, T., 2020. Decreased RPM reduces von Willebrand factor degradation with the EVAHEART LVAS: implications for device-specific LVAD management. Journal of cardiac surgery 35, 1477-1483.

Bieritz, S., 2020. Resolving flow properties of spiral groove bearings to improve mechanical circulatory support hemopatibility. PhD thesis published online: Rice University Electronic Theses and Dissertations.

Blackshear, P.L., Jr., Dorman, F.D., Steinbach, J.H., Maybach, E.J., Singh, A., Collingham, R.E., 1966. Shear, wall interaction and hemolysis. Transactions - American Society for Artificial Internal Organs 12, 113-120.

Bourque, K., Cotter, C., Dague, C., Harjes, D., Dur, O., Duhamel, J., Spink, K., Walsh, K., Burke, E., 2016. Design Rationale and Preclinical Evaluation of the HeartMate 3 Left Ventricular Assist System for Hemocompatibility. ASAIO journal (American Society for Artificial Internal Organs : 1992) 62, 375-383.

Chan, C.H.H., Inoue, M., Ki, K.K., Murashige, T., Fraser, J.F., Simmonds, M.J., Tansley, G.D., Watanabe, N., 2020. Shear-dependent platelet aggregation size. Artificial organs 44, 1286-1295.

Chan, C.H.H., Pieper, I.L., Robinson, C.R., Friedmann, Y., Kanamarlapudi, V., Thornton, C.A., 2017. Shear Stress-Induced Total Blood Trauma in Multiple Species. Artificial organs 41, 934-947.

Chan, C.H.H., Simmonds, M.J., Fraser, K.H., Igarashi, K., Ki, K.K., Murashige, T., Joseph, M.T., Fraser, J.F., Tansley, G.D., Watanabe, N., 2022. Discrete responses of erythrocytes, platelets, and von Willebrand factor to shear. Journal of biomechanics 130, 110898.

Crow, S., Chen, D., Milano, C., Thomas, W., Joyce, L., Piacentino, V., 3rd, Sharma, R., Wu, J., Arepally, G., Bowles, D., Rogers, J., Villamizar-Ortiz, N., 2010. Acquired von Willebrand syndrome in continuous-flow ventricular assist device recipients. The Annals of thoracic surgery 90, 1263-1269; discussion 1269.

Crow, S., John, R., Boyle, A., Shumway, S., Liao, K., Colvin-Adams, M., Toninato, C., Missov, E., Pritzker, M., Martin, C., Garry, D., Thomas, W., Joyce, L., 2009.

Gastrointestinal bleeding rates in recipients of nonpulsatile and pulsatile left ventricular assist devices. The Journal of thoracic and cardiovascular surgery 137, 208-215.
Daily J, W., Nece R, E., 1960. Chamber dimension effects on induced flow and frictional resistance of enclosed rotating disks. Journal of Basic Engineering 82, 217-232.
Fåhræus, R., Lindqvist, T., 1931. The viscosity of the blood in narrow capillary tubes. American Journal of Physiology 96, 562-568.
Fu, Y., Hu, Y., Huang, F., Zhou, M., 2019. The Impact of Pulsatile Flow on Suspension Force for Hydrodynamically Levitated Blood Pump. Journal of healthcare engineering 2019, 8065920.
Huisjes, R., Bogdanova, A., van Solinge, W.W., Schiffelers, R.M., Kaestner, L., van Wijk, R., 2018. Squeezing for Life - Properties of Red Blood Cell Deformability. Frontiers in physiology 9, 656.
James, N.L., Wilkinson, C.M., Lingard, N.L., van der Meer, A.L., Woodard, J.C., 2003. Evaluation of hemolysis in the VentrAssist implantable rotary blood pump. Artificial organs 27, 108-113.
Kink, T., Reul, H., 2004. Concept for a new hydrodynamic blood bearing for miniature blood pumps. Artificial organs 28, 916-920.
Kirklin, J.K., Naftel, D.C., Pagani, F.D., Kormos, R.L., Stevenson, L.W., Blume, E.D., Myers, S.L., Miller, M.A., Baldwin, J.T., Young, J.B., 2015. Seventh INTERMACS annual report: 15,000 patients and counting. The Journal of heart and lung transplantation : the official publication of the International Society for Heart Transplantation 34, 1495-1504.
Kosaka, R., Sakota, D., Nishida, M., Maruyama, O., Yamane, T., 2021. Improvement of hemolysis performance in a hydrodynamically levitated centrifugal blood pump by optimizing a shroud size. Journal of artificial organs : the official journal of the Japanese Society for Artificial Organs 24, 157-163.
Krabatsch, T., Netuka, I., Schmitto, J.D., Zimpfer, D., Garbade, J., Rao, V., Morshuis, M., Beyersdorf, F., Marasco, S., Damme, L., Pya, Y., 2017. Heartmate 3 fully magnetically levitated left ventricular assist device for the treatment of advanced heart failure -1 year results from the Ce mark trial. Journal of cardiothoracic surgery 12, 23.
Leslie, L.J., Marshall, L.J., Devitt, A., Hilton, A., Tansley, G.D., 2013. Cell exclusion in couette flow: evaluation through flow visualization and mechanical forces. Artificial organs 37, 267-275.
Leverett, L.B., Hellums, J.D., Alfrey, C.P., Lynch, E.C., 1972. Red blood cell damage by shear stress. Biophysical journal 12, 257-273.
Malinauskas, R.A., Hariharan, P., Day, S.W., Herbertson, L.H., Buesen, M., Steinseifer, U., Aycock, K.I., Good, B.C., Deutsch, S., Manning, K.B., Craven, B.A., 2017. FDA Benchmark Medical Device Flow Models for CFD Validation. ASAIO

journal (American Society for Artificial Internal Organs : 1992) 63, 150-160.
Mehra, M.R., Goldstein, D.J., Uriel, N., Cleveland, J.C., Jr., Yuzefpolskaya, M., Salerno, C., Walsh, M.N., Milano, C.A., Patel, C.B., Ewald, G.A., Itoh, A., Dean, D., Krishnamoorthy, A., Cotts, W.G., Tatooles, A.J., Jorde, U.P., Bruckner, B.A., Estep, J.D., Jeevanandam, V., Sayer, G., Horstmanshof, D., Long, J.W., Gulati, S., Skipper, E.R., O'Connell, J.B., Heatley, G., Sood, P., Naka, Y., 2018. Two-Year Outcomes with a Magnetically Levitated Cardiac Pump in Heart Failure. The New England journal of medicine 378, 1386-1395.
Mehra, M.R., Naka, Y., Uriel, N., Goldstein, D.J., Cleveland, J.C., Jr., Colombo, P.C., Walsh, M.N., Milano, C.A., Patel, C.B., Jorde, U.P., Pagani, F.D., Aaronson, K.D., Dean, D.A., McCants, K., Itoh, A., Ewald, G.A., Horstmanshof, D., Long, J.W., Salerno, C., 2017. A Fully Magnetically Levitated Circulatory Pump for Advanced Heart Failure. The New England journal of medicine 376, 440-450.
Molina, E.J., Shah, P., Kiernan, M.S., Cornwell, W.K., 3rd, Copeland, H., Takeda, K., Fernandez, F.G., Badhwar, V., Habib, R.H., Jacobs, J.P., Koehl, D., Kirklin, J.K., Pagani, F.D., Cowger, J.A., 2021. The Society of Thoracic Surgeons Intermacs 2020 Annual Report. The Annals of thoracic surgery 111, 778-792.
Murashige, T., Kosaka, R., Sakota, D., Nishida, M., Kawaguchi, Y., Yamane, T., Maruyama, O., 2015. Evaluation of a Spiral Groove Geometry for Improvement of Hemolysis Level in a Hydrodynamically Levitated Centrifugal Blood Pump. Artificial organs 39, 710-714.
Murashige, T., Sakota, D., Kosaka, R., Nishida, M., Kawaguchi, Y., Yamane, T., Maruyama, O., 2016. Plasma Skimming in a Spiral Groove Bearing of a Centrifugal Blood Pump. Artificial organs 40, 856-866.
Rogers, J.G., Pagani, F.D., Tatooles, A.J., Bhat, G., Slaughter, M.S., Birks, E.J., Boyce, S.W., Najjar, S.S., Jeevanandam, V., Anderson, A.S., Gregoric, I.D., Mallidi, H., Leadley, K., Aaronson, K.D., Frazier, O.H., Milano, C.A., 2017. Intrapericardial Left Ventricular Assist Device for Advanced Heart Failure. The New England journal of medicine 376, 451-460.
Schneider, S.W., Nuschele, S., Wixforth, A., Gorzelanny, C., Alexander-Katz, A., Netz, R.R., Schneider, M.F., 2007. Shear-induced unfolding triggers adhesion of von Willebrand factor fibers. Proceedings of the National Academy of Sciences of the United States of America 104, 7899-7903.
Smeets, M.W.J., Mourik, M.J., Niessen, H.W.M., Hordijk, P.L., 2017. Stasis Promotes Erythrocyte Adhesion to von Willebrand Factor. Arteriosclerosis, thrombosis, and vascular biology 37, 1618-1627.
Uriel, N., Colombo, P.C., Cleveland, J.C., Long, J.W., Salerno, C., Goldstein, D.J., Patel, C.B., Ewald, G.A., Tatooles, A.J., Silvestry, S.C., John, R., Caldeira, C., Jeevanandam, V., Boyle, A.J., Sundareswaran, K.S., Sood, P., Mehra, M.R., 2017. Hemocompatibility-Related Outcomes in the MOMENTUM 3 Trial at 6

Months: A Randomized Controlled Study of a Fully Magnetically Levitated Pump in Advanced Heart Failure. Circulation 135, 2003-2012.

Figures and Table

Figure 1. Experimental setup. a) A custom-built test rig. The device comprises a motor, a force sensor, a rotating geometry either spiral groove bearing (SGB) or grooveless disc, a blood reservoir and a translation stage. The circulation loop has a blood sampling port and a flow sensor. b) Ridge and groove patterns inside the SGB. h_{gap} = shearing gap between the bottom surface of blood reservoir and the ridge surface; h_{groove} = groove depth of 200 μm + h_{gap}; τ_{ridge} = gap shear stress; τ_{groove} = groove shear stress.

Figure 2. Shear-induced haemolysis between the spiral groove bearing (SGB) and grooveless disc in different shearing gaps of 20, 30 and 40 μm after an hour. Results expressed as mean ± standard deviation. ***P < 0.001, ****P < 0.0001.

Figure 3. The haemolysis results of same flow rate of 50 mL/min in two different gap-clamp conditions: 20 μm gap with a clamp and 30 μm gap without a clamp after two hours. Results expressed as mean ± standard deviation.

Figure 4a. Classification of the vWF multimers was performed using agarose gel electrophoresis. Bands 1 to 5 (bottom dotted box) from the dye front of the electrophoretic strip were classified as low molecular weight von Willebrand factor multimers (LMW vWF), bands 6 to 10 as intermediate molecular weight von Willebrand factor multimers and all those > band 10 (top dotted box) as high molecular weight von Willebrand factor multimers (HMW vWF). **Figure 4b.** Shear-induced HMW vWF multimer degradation. Blood was subjected to different shearing gaps ranging from 20-40 μm after an hour in a custom-built test rig. **Figure 4c.** Shear-induced LMW vWF multimer accumulation. Results expressed as mean ratio ± standard deviation of post-shear sample to the baseline sample in each shear gap. *P < 0.05.

Figure 5. Velocity streamline plot of flow injected at the entrance to the bearing. Primary flows are displayed travelling along the grooves with secondary flows migrating from the ridge to the groove region.

Figure 6. Shear stress contour plot along a groove and ridge cross section. Higher shear stresses at the ridge regions in comparison to the groove regions.

Figure 7. A surface-shear stress analysis image of the Spiral Groove Bearing.

565 **Table 1.** Spiral groove bearing gaps, calculated maximum shear stresses at ridge and
566 groove, measured volumetric flow rates, calculated Reynolds numbers at ridge and
567 groove regimes.

Figure

Click here to access/download;Figure;Figure_revision_3rd rev.pdf

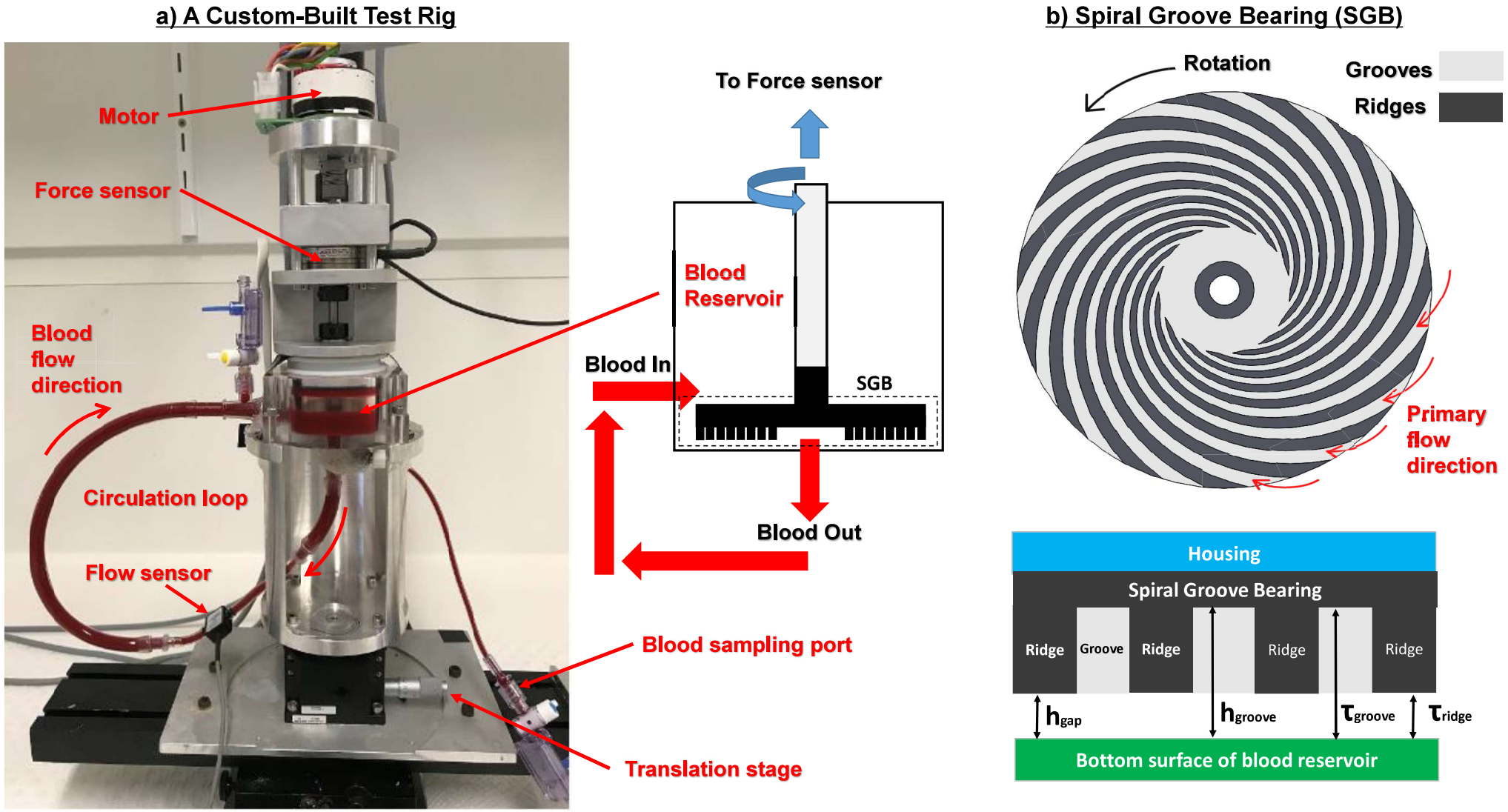

Figure 1.

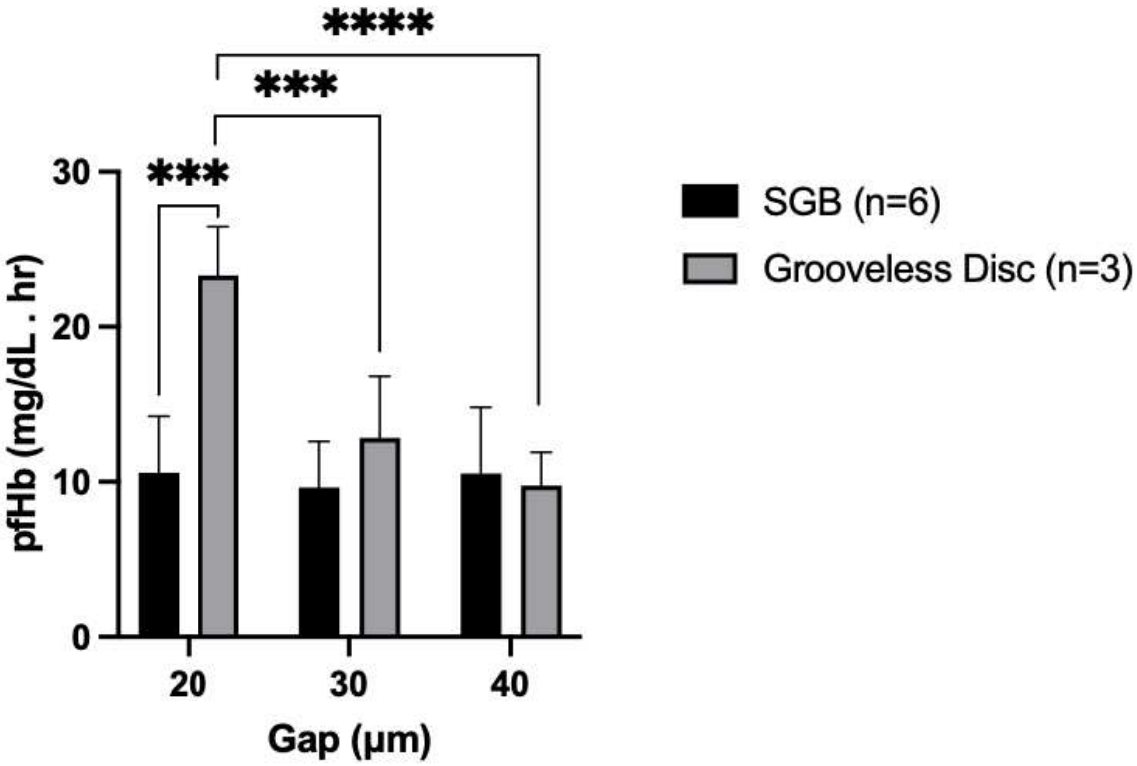

Figure 2.

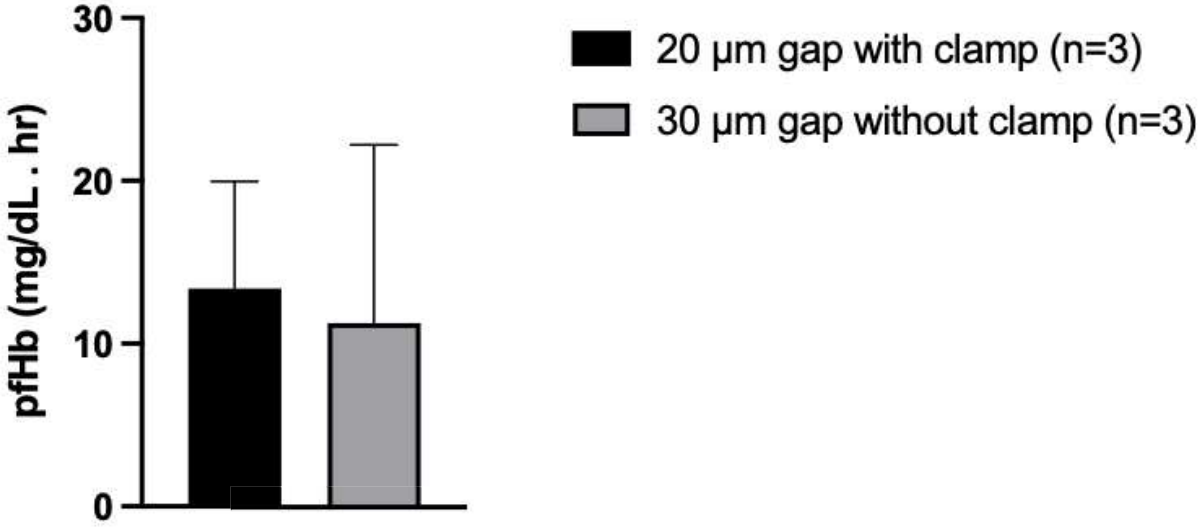
30
20
10
0
pfHb (mg/dL . hr)
20 µm gap with clamp (n=3)
30 µm gap without clamp (n=3)

Figure 3.

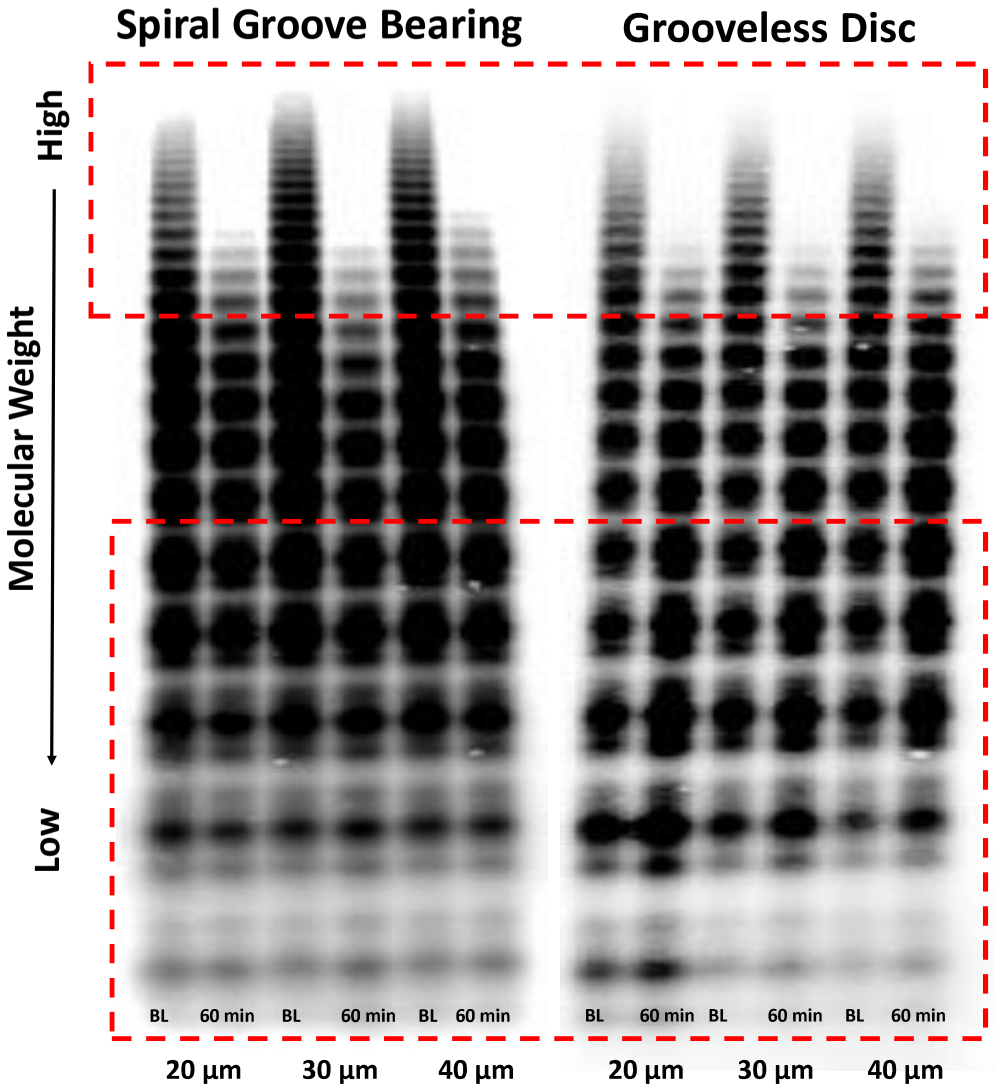

Figure 4a.

HMW vWF multimers (> band 10)

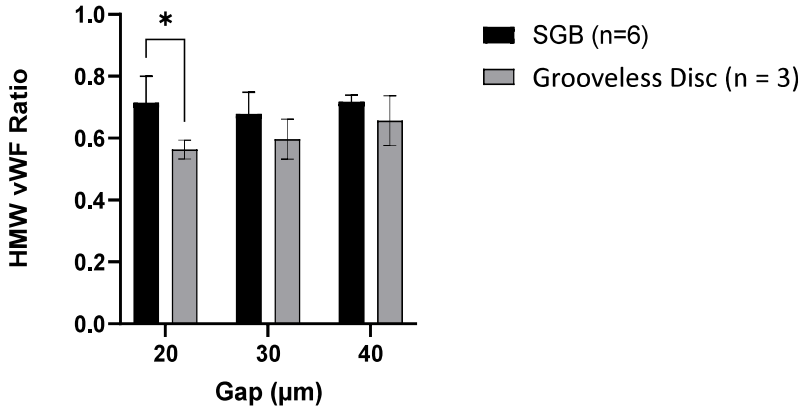

Figure 4b.

LMW vWF multimers (band 1-5)

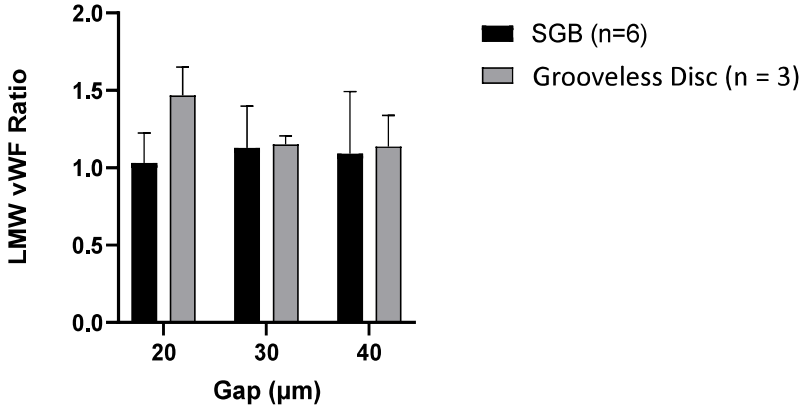

Figure 4c.

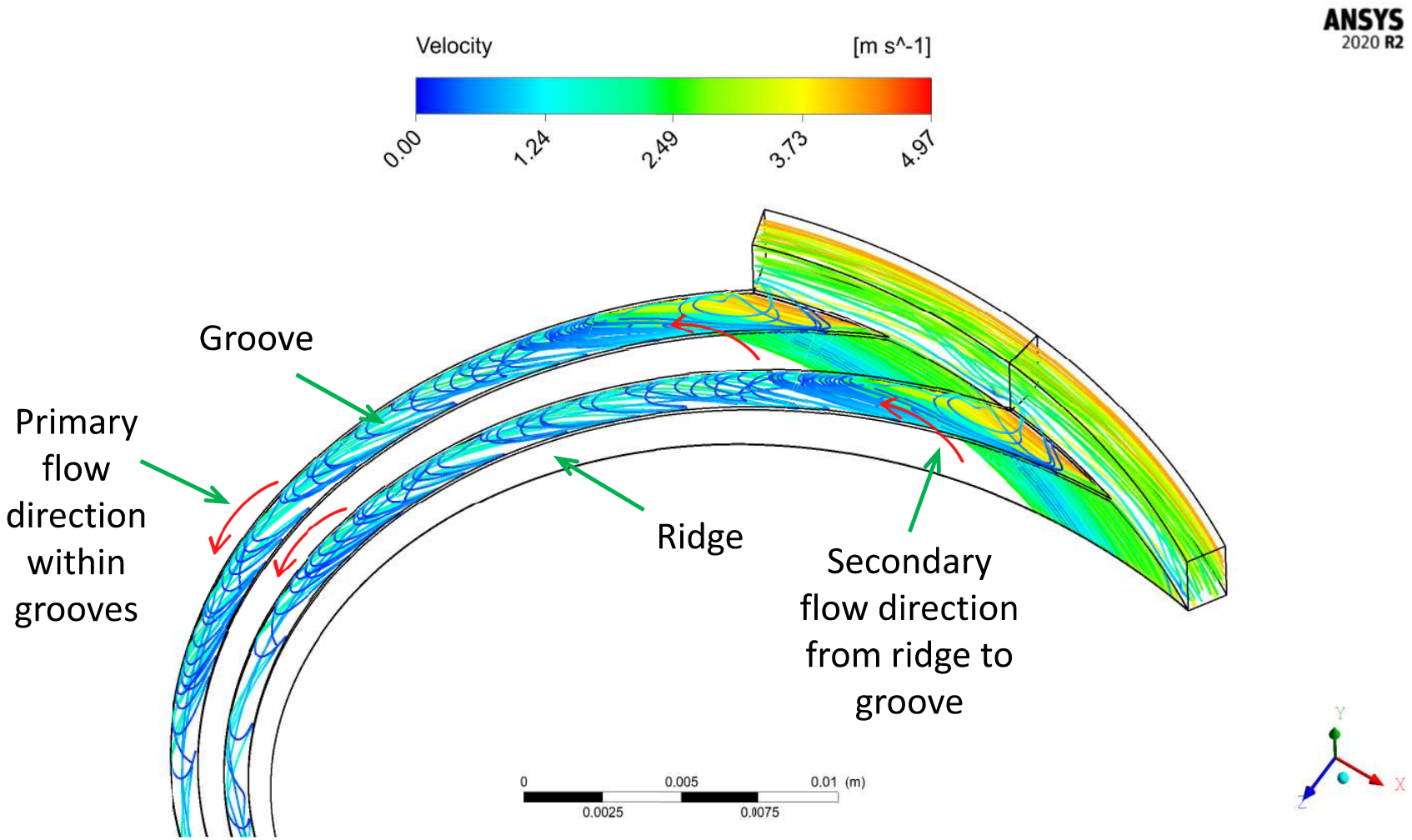
ANSYS
2020 R2
Velocity
[m s^-1]
0.00
1.24
2.49
3.73
4.97
Groove
Primary flow direction within grooves
Ridge
Secondary flow direction from ridge to groove
0
0.005
0.01 (m)
0.0025
0.0075
Y
X
Z

Figure 5.

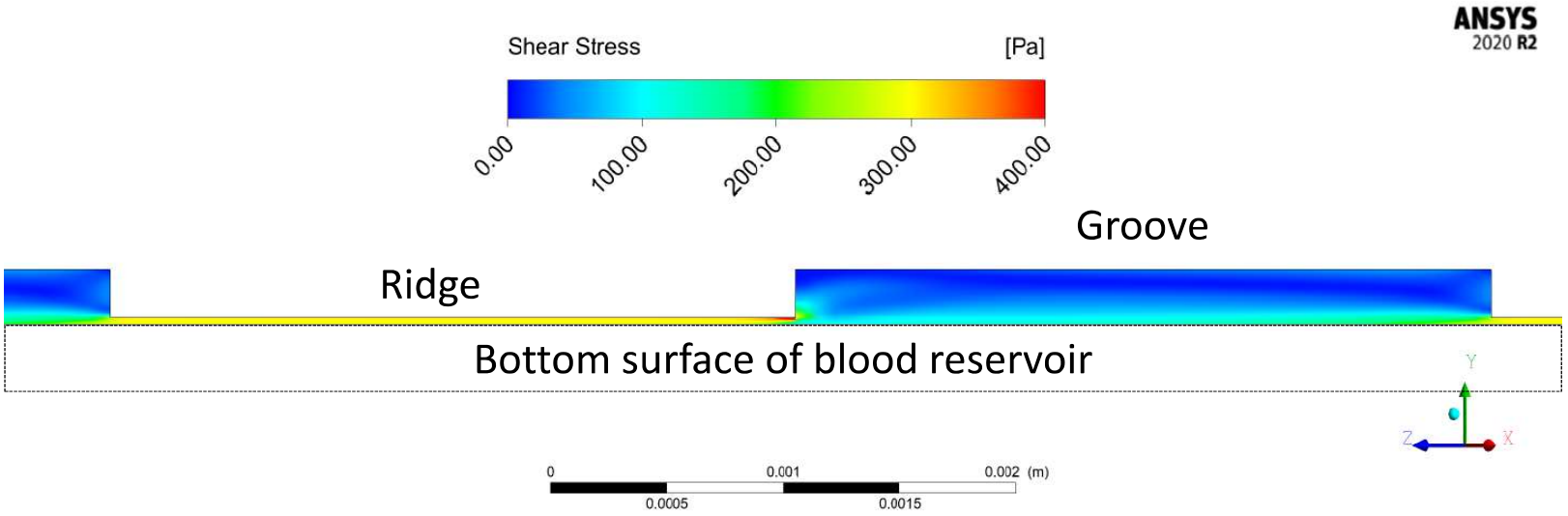
ANSYS
2020 R2
Shear Stress
[Pa]
0.00
100.00
200.00
300.00
400.00
Groove
Ridge
Bottom surface of blood reservoir
Y
Z
X
0
0.001
0.002 (m)
0.0005
0.0015

Figure 6.

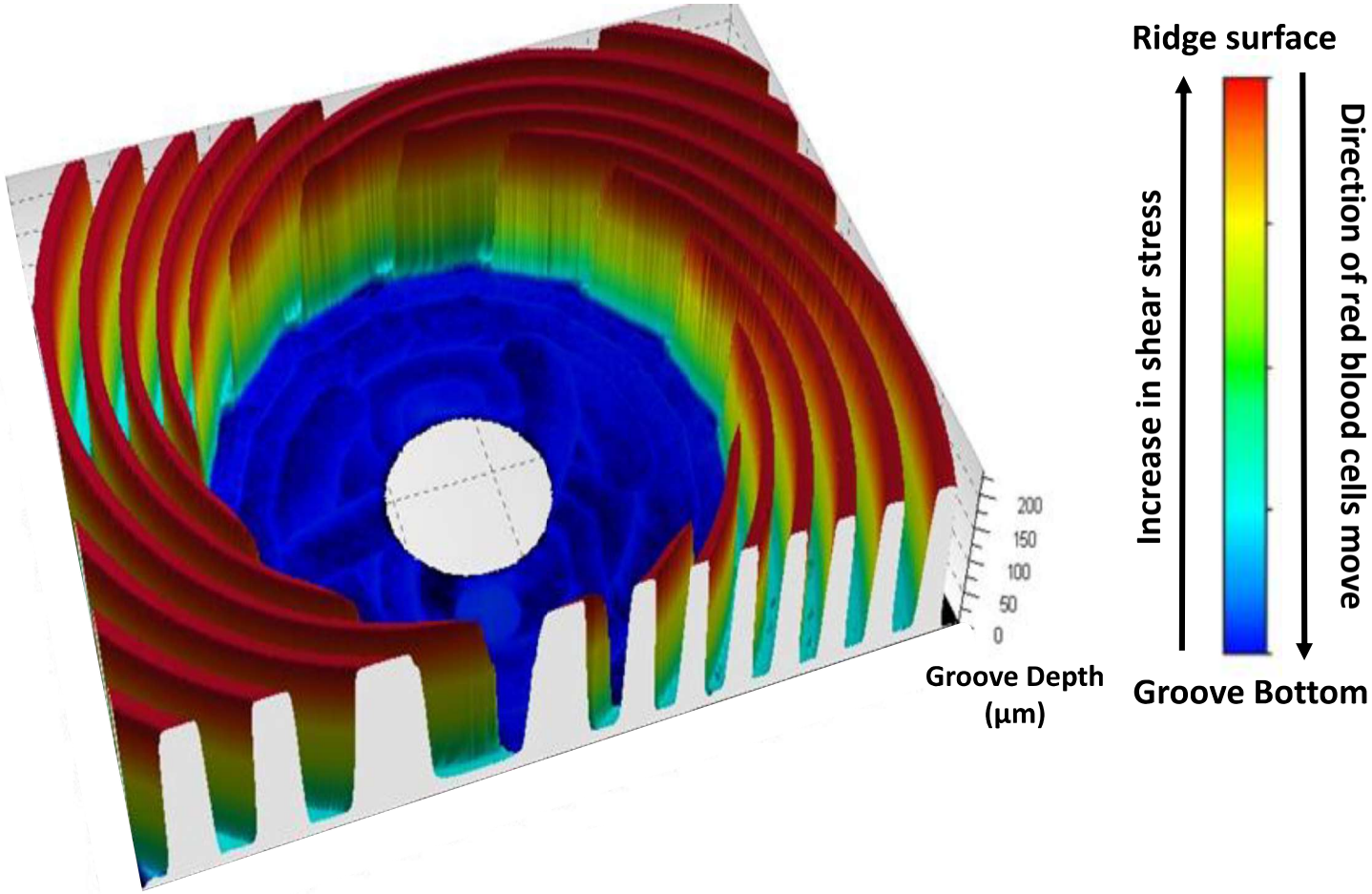
200
150
100
50
0
Groove Depth
(µm)
Ridge surface
Increase in shear stress
Direction of red blood cells move
Groove Bottom

Figure 7.

Spiral groove bearing gap, h_{gap} (μm)	20	30	40
Maximum ridge surface shear stress, τ_{ridge} (Pa)	704	469	352
Maximum groove shear stress, τ_{groove} (Pa)	64	61	59
Volumetric flow rate, Q_{gap} (mL/min)	60	50	40
Re_{ridge} (Critical Reynolds number > 300,000)	148,525	148,525	148,525
Re_{groove} (Critical Reynolds number > 2,300)	27	23	19

Table 1.

Conflict of Interest Statement

The authors have no conflicts of interest to declare.